Structure-informed classification of RyR1 variants highlights limitations of current predictors and enables clinical interpretation

Rolando Hernández Trapero, Mihaly Badonyi & Joseph A Marsh*

MRC Human Genetics Unit, Institute of Genetics & Cancer, University of Edinburgh, Edinburgh EH4 2XU, UK

**joseph.marsh@ed.ac.uk*

Abstract

RyR1-related disorders, arising from variants in the RYR1 gene encoding the skeletal muscle ryanodine receptor, encompass a wide range of dominant and recessive phenotypes. The extensive length of RyR1 and diverse mechanisms underlying disease variants pose significant challenges for clinical interpretation, exacerbated by the limited performance and biases of current variant effect predictors (VEPs). This study evaluates the efficacy of 70 VEPs for distinguishing pathogenic RyR1 missense variants from putatively benign variants derived from population databases. Existing VEPs show variable performance. Those trained on known clinical labels show greater classification performance, but this is likely heavily inflated by data circularity. In contrast, VEPs using methodologies that avoid or minimise training bias show limited performance, likely reflecting difficulty in identifying gain-of-function variants. Leveraging protein structural information, we introduce Spatial Proximity to Disease Variants (SPDV), a novel metric based solely on three-dimensional clustering of pathogenic mutations. We determine ACMG/AMP PP3/BP4 classification thresholds for our method and top-performing VEPs, allowing us to assign PP3/BP4 evidence levels to all available RyR1 missense VUSs in ClinVar. Thus, we suggest that our protein-structure based approach represents an orthogonal strategy over existing computational tools for aiding in the diagnosis of RyR1-related diseases.

Introduction

RyR1, encoded by the *RYR1* gene, is the skeletal muscle ryanodine receptor and the largest human ion channel, with a sequence spanning 5038 amino acids and a molecular weight of ~2.2 MDa (1, 2). The protein serves as a calcium release channel of the sarcoplasmic reticulum, as well as a bridging structure connecting the sarcoplasmic reticulum and transverse tubule. The monomeric subunits self-associate to form homotetrameric assemblies involved in excitation-contraction (EC) coupling. Four-fifths of the RyR1 protein is cytoplasmic and the remaining one-fifth consists of lumenal and membrane spanning domains (3). Small molecule ligands to RyR1 include Ca^{2+}, ATP, and caffeine, along with several pharmaceuticals such as volatile anaesthetics (*e.g.,* halothane), ryanodine (channel agonist), and dantrolene (channel antagonist) (4-6).

Mutations in RyR1 can cause a highly heterogeneous set of genetic disorders (6-8). Pathogenic RyR1 variants occur across the sequence and may disrupt regulatory interactions, hypersensitizing the protein to lower voltage thresholds, or cause gain or loss of function through other mechanisms (6). Malignant hyperthermia (MH) is an autosomal dominant disorder that can be explained by increased probability of channel opening due to a reduction in the threshold needed for calcium induced calcium release. This leads to leaky channels under high temperatures or exposure to triggering agents, such as volatile anaesthetics, muscle relaxants, and caffeine. Dominant variants can also cause central core disease (CCD) due either to receptor hypersensitization, resulting in calcium dysregulation and depletion of calcium stores even under resting conditions, or affecting the voltage-dependent activation of calcium release (EC uncoupling) (9-11). Unusually, central core/rod disease (CCRD) can result from excessive production of RyR1 (12). In contrast, recessive mutations that cause multi-minicore disease (MmD), centronuclear myopathy (CNM) and congenital fiber-type disproportion (CFTD) reduce RyR1 expression or activity, *i.e.,* cause a loss of function. However, with such diversity in pathologies stemming from variants in one protein, it is possible that RyR1 disorders could be best considered as occurring in a phenotypic spectrum, as a single disease with varying manifestations (13-16).

A major issue that arises when attempting to diagnose RyR1-related diseases is the huge number of variants of uncertain significance (VUSs) that are identified. The extreme length of the *RYR1* gene means that the chances of finding one or more VUSs when sequencing the gene in a patient is very high. Upon identification of a VUS, a patient will often be referred for further testing. Especially in the case of malignant hyperthermia, the *in vitro* contracture test (IVCT) can be useful for diagnosis in the event of finding a VUS in a clinical panel (17). However, this solution has its disadvantages, as it is done on a per-patient basis without the

purpose of providing mechanistic insight. Furthermore, a negative IVCT does not preclude the occurrence of a different but related RyR1 dysfunction. Thus, if computational approaches could be used to better exclude VUSs that have little chance of having clinically meaningful effects, or prioritise those with a high likelihood of pathogenicity, this could have a significant benefit in terms of improving diagnosis and reducing the burden of patient testing.

Variant effect predictors (VEPs) are computational tools for scoring the likely damaging effects or pathogenicity of genetic variants. Compared to the experimental characterization of variants, these have the advantage of being very fast and essentially free to run. However, given the large number of VEPs that have been released, it can be difficult to know what the best methods are to use. Moreover, the performance of new VEPs as reported upon publication tends to be highly overstated (18), and thus the extent to which their predictions can be relied upon is often unclear. The performance of VEPs can also vary dramatically between different genes, with their utility being markedly worse for genes associated with dominant-negative and gain-of-function molecular mechanisms (19). Given that the extensive experimental evidence for gain-of-function effects in RyR1 (9, 10, 20-22) along with recent computational predictions showing that, overall, pathogenic RyR1 variants were most likely to be associated with gain-of-function effects (23), this suggest that current VEPs might struggle with them.

In this study, we have performed an analysis of known missense variants in RyR1, with the goal of improving our ability to computationally predict their effects. First, we evaluate currently available VEPs for their ability to distinguish between pathogenic and putatively benign variants. While certain clinical-trained methods appear to perform well, we find that this is likely due to data circularity that arises from these methods having been trained using known RyR1 variants. In contrast, population-free VEPs, which are free from this bias, show substantially worse performance. Next, we investigate the protein structural context of RyR1 missense variants. While we find that the effects of variants on protein stability have little power to explain pathogenicity, consistent with a likely gain-of-function disease mechanism, we observe strong clustering of pathogenic missense variants within three-dimensional space. Based upon this, we introduce a new method, based solely on spatial proximity to known pathogenic mutations, which we show performs comparably to the best population-free VEPs for the identification of pathogenic missense variants in RyR1. Thus, our structure-based approach holds complementary value to existing computational tools for aiding the diagnosis of RyR1-related disorders.

Results and Discussion

Compilation of known RyR1 missense variants

To obtain a set of pathogenic RyR1 missense variants to use for our analyses, we compiled disease-associated missense variants from the ClinVar, OMIM, and dbSNP databases, as well as performing an extensive search of the literature for other reported cases. In total we identified 425 missense variants that have been reported to be associated with RyR1 disease, which are listed in **Table S1**. This approach gives far more disease-associated RyR1 variants than the 85 pathogenic and likely pathogenic missense variants classified with strict criteria used by the ClinGen Variant Curation Expert Panel (VCEP) (24). While we expect that there will inevitably be some false positive cases in our disease-associated variant dataset, given the less stringent selection criteria compared to the VCEP, we think that the increased statistical power afforded by the much larger dataset is worth the trade-off.

Within our set of disease-associated missense variants, we were able to further classify these based upon clinical phenotypes: 162 associated with autosomal dominant malignant hyperthermia (MH), 70 with autosomal dominant central core disease (CCD), 124 with other autosomal dominant RYR1-related disease (RRD), and 68 with autosomal recessive RYR1-related disease. The RRD group was introduced because the RYR1 disease spectrum includes highly heterogeneous and rare disease phenotypes, which cannot be reasonably evaluated if taken as individual groups. Recessive RyR1-related disease variants were also treated separately to investigate differences that might arise between this group and dominantly inherited disease variants. The distribution of these four classes of missense variants along the linear sequence of the RyR1 protein is shown in **Figure 1**.

For comparison, we also identified 6254 missense variants present in the human population using gnomAD v4.1, after excluding any present in our disease-associated dataset. We consider missense variants present in gnomAD at any allele frequency, excluding those from our pathogenic set, to be “putatively benign” for the purpose of analysing VEP performance, as we have done in several recent studies (19, 25-31), as an allele frequency filter would severely reduce the number of variants in our analysis. Furthermore, it has been argued that assessing performance against rare variants present in the population is more reflective of the practical clinical utilisation of computational predictors, in which rare pathogenic variants must be distinguished from rare benign variants (31, 32). As gnomAD is derived from a generally healthy population, we expect that the vast majority of these variants should have no clinically relevant effect, although we accept that it could contain some recessive variants

in a heterozygous state, or variants associated with later onset disease or with incomplete penetrance (33).

Evaluation of variant effect predictors for discriminating between disease-associated and putatively benign missense variants

Next, we sought to evaluate the performance of currently available VEPs at distinguishing between dominant pathogenic and putatively benign missense variants. We excluded recessive variants from this analysis, as they are frequently found in a heterozygous state in the healthy population. We therefore computed predicted effects of the available RyR1 missense variants using 70 different VEPs, mostly from our recent benchmarking study (31). To evaluate the performance of the VEPs as classifiers, we used receiver operating characteristic (ROC) curves and calculated their area under the curve (AUC) values. This approach is widely used for assessing binary classifiers (34) and is robust to differences in dataset size, which is important given that not all predictors return scores for every variant.

The variant effect predictors (VEPs) can be grouped into three classes based on their exposure to human-derived data and the resulting risk of circularity (35). *Clinical-trained* VEPs are supervised machine learning models—often using random forests or neural networks—that are explicitly trained on variants with clinical labels (*e.g.*, pathogenic and benign). As a result, they are highly susceptible to data circularity, particularly when performance is assessed on variants from the same or similar sources (36-38). In our case, since we analyse all known *RYR1* missense variants, it is almost certain that many of these were included in the training data for clinical-trained predictors. As a result, the apparent performance of these methods on *RYR1* will likely be inflated due to overlap between training and evaluation data.

In contrast, *population-free* VEPs do not use clinical or population-derived variants during training and thus are almost completely immune from circularity concerns. These methods typically rely on features such as evolutionary conservation derived from multiple sequence alignments (39), or increasingly, utilise protein language models (40). Notably, deep mutational scanning (DMS)–based benchmarking, which provides independent ground truth, has consistently found that many of the top-performing VEPs tend to be population-free (35). While it is possible that clinical-trained VEPs developed specifically for prioritising clinically relevant variants will have some advantages at that task compared to unsupervised methods, the greatly reduced bias of population-free VEPs means we can have much more confidence in their reported performance.

Finally, certain predictors—while not explicitly trained on clinical labels—are nonetheless tuned or calibrated using population data, such as allele frequencies. These *population-*

tuned VEPs, including tools like AlphaMissense (41), exhibit reduced circularity issues compared to clinical-trained methods, but are not fully independent and may still exhibit performance inflation when tested on variants drawn from human population or clinical datasets (35, 42).

Interestingly, we observe the top 13 performing VEPs when assessing their ability to discriminate between pathogenic and putatively benign RyR1 missense variants to be clinical-trained methods (**Figure 2**; **Table S2**). The best performance is seen for the metapredictor BayesDel_noAF (ROC AUC: 0.874) (43). Notably, this is much better performance than observed for VARITY_R (ROC AUC: 0.789) (32), which was previously identified as the top performing clinical-trained VEP when benchmarked against independent DMS data (35), and also showed very low bias when applied to variants from different ancestry groups (42). Given that VARITY_R was designed in a manner to minimise training bias and that BayesDel_noAF underperformed compared to VARITY_R in the benchmark, this strongly suggests that the apparent top performance of BayesDel_noAF here against RyR1 variants is inflated by circularity, having been trained directly on many of the known variants in our test set. We also note the strong ancestry bias recently observed by BayesDel_noAF (42), further supporting the role of circularity.

Among the population-free VEPs, the highest ROC AUC is achieved by PHACT (44) (ROC AUC: 0.805). Interestingly, this method did not stand out in the recent DMS-based benchmark, ranking 41st out of 97 tested VEPs (35). Therefore, it is possible its performance here represents an element of random chance. Alternatively, we could speculate that perhaps PHACT uses high quality sequence alignments for RyR1, which may be difficult for other methods to align effectively due to the gene's large size. Interestingly, the top performing VEP in that study, CPT, which combines sequence alignments, language models and protein structure (45), obtains a ROC AUC of only 0.748. AlphaMissense, a population-tuned predictor that ranked 2nd (behind CPT) in the recent benchmark, achieved a ROC AUC of 0.796. While it avoids clinical label training, its reliance on population data introduces some risk of mild circularity.

Overall, the performance reported here as measured by ROC AUC values, appears to be fairly weak. In part, this may be related to the previous observation that gain-of-function missense variants are poorly predicted by current VEPs. Notably, the performance here is on a very similar level as reported for gain-of-function variants in that study. For example, DeepSequence (46) (the top-ranking population-free VEP considered in that study) was found shown to have an average ROC AUC of 0.86 for genes with loss-of-function disease mechanisms and 0.80 for genes with gain-of-function disease mechanisms when

discriminating between pathogenic ClinVar and putatively benign gnomAD missense variants (19), very similar to the datasets utilised here. This is slightly lower but similar to the ROC AUC of 0.780 observed for DeepSequence here.

We also considered whether predictive performance might be different for variants associated with different dominant disease phenotypes. When performing assessments on a per-phenotype basis (*e.g.,* discrimination between MH and gnomAD missense variants), the relative performance of most VEPs changes very little, with the same few clinical-trained methods ranking best across all three groups (**Figure S1**). However, it does appear that MH are less well predicted than those associated with CCD and RRD. For example, CPT has a ROC AUC of 0.678 on the MH subset, compared to 0.822 and 0.798 for the CCD and RRD subsets. Since MH is an exposure-dependent genetic disorder, it is likely underdiagnosed relative to CCD and RRD, and its associated variants may exert weaker effects on fitness. As a result, they may be more difficult for computational predictors to identify.

Protein structural analysis of Ryr1 missense variants

Most VEPs in this study utilise only protein sequence information, with no inclusion of three-dimensional protein structures (47). Given the limitations of current VEPs for the identification of pathogenic missense variants in RyR1, we wondered whether consideration of protein structural information could help us to improve upon this.

Previously, it has been shown that predicted changes in protein stability can be useful for the identification of pathogenic missense variants in some proteins (27), particularly those associated with recessive disorders and haploinsufficiency (19, 48). Therefore, we first assessed whether the predicted effects of missense variants on protein stability showed any difference between pathogenic and putatively benign variants, or between the different phenotypic classes. We use FoldX (49) to predict changes in the Gibbs free energy (ΔΔG) between wild-type and mutant structures, considering both intra- and intermolecular effects calculated from the full tetrameric complex. We considered absolute (|ΔΔG|) values from the full protein complex structure as these tend to show the largest differences between pathogenic and putatively benign mutations (19, 50). Notably, |ΔΔG| showed essentially no ability to discriminate between pathogenic and putatively benign RyR1 missense variants, with a ROC AUC value of 0.557. The only significant differences were between putatively benign variants and RRD variants ($P = 7.2 \times 10^{-5}$, Wilcoxon rank-sum test), as well as MH and RRD ($P = 0.02$, Wilcoxon rank-sum test) (**Figure S2**). The MH variants had a lower |ΔΔG| than the more heterogeneous RRD variants, which is consistent with the fact that this phenotypic category's mechanism of disease is gain of function, which tend to not be structurally disruptive (19). In contrast, the heterogeneous RRD group is expected to include

some loss of function variants, which are expected to have higher ΔΔG values than benign and therefore likely to be structurally disruptive. However, our results suggest that protein destabilisation or disruption of inter-subunit interactions is not a major contributor to any class of RyR1 pathogenic variants, especially given its poor performance in variant classification.

In previous work from our group, it was found that pathogenic gain-of-function and dominant-negative variants show a strong tendency to cluster in three-dimensional space; it was therefore suggested that this clustering could potentially be used to improve the predictions of mutations associated with such non-loss-of-function mechanisms (19). Since previous work suggests that most dominant RyR1 variants are associated with gain-of-function effects (6), which is further supported by our ΔΔG analysis, we next decided to assess the level of mutation clustering in RyR1.

Some evidence for clustering of pathogenic RyR1 missense variants is immediately apparent when inspecting the one-dimensional sequence-level plot in **Figure 1**, most notably with the high density of variants near the C terminus, particularly those associated with CCD. When we plot the positions of these mutations onto the structure of the RyR1 tetramer (**Figure 3**), the clustering around the C-terminal pore region becomes even clearer. Additionally, we can see that distinct placements emerge gathered around the N terminus, the middle of the sequence, and the C terminus. We note the enrichments of these variants in the MIR (protein mannosyltransferase, IP3R, and RyR) domains at the N terminus of the sequence (51). Specifically, based on these clustering analyses, MH variants mostly clustered in the Nsol, Bsol, pVSD, pore, and CTD domains, CCD variants clustered in the pVSD, pore, and CTD domains, RRD variants clustered in the NTD, Nsol, pore, and CTD, while recessive variants were spread across the structure (5, 52, 53). Interestingly, we see that CCD variants cluster most strongly in the C terminus at the lower extreme of the protein complex, which corresponds to the channel and activation (CAC) domains. This is mechanistically interesting, as CCD is thought to occur due to incomplete closure of the ion channel, thus resulting in permanent leakage of calcium. The MH variants are also shown to cluster around the CTD, which has been shown to harbour a Ca^{2+} binding site, as well as an allosteric tryptophan residue (W4716), which is mechanistically interesting as in malignant hyperthermia, as hypersensitivity to Ca^{2+} activation is one of its causative mechanisms (54-56).

To quantify the degree of spatial clustering of pathogenic variants, we used the recently introduced Extent of Disease Clustering (EDC) metric (19). EDC values close to one indicate little-to-no spatial clustering of the sites of pathogenic mutations, *i.e.,* the sites of disease

variants are essentially randomly dispersed throughout the protein. In contrast, EDC values greater than one indicate that the pathogenic mutations are clustered in three-dimensional space. Previously, the mean EDC value for pathogenic missense variants in autosomal recessive disease genes was 1.02, indicating very little tendency to cluster (19). In contrast, gain-of-function and dominant-negative missense variants from autosomal dominant disease genes both had mean EDC values of 1.27, demonstrating their strong tendency to cluster together.

For RyR1, when we consider all pathogenic missense variants collectively, we obtain an EDC value of 1.16, indicative of moderate clustering and consistent with a mixture of gain- and loss-of-function mechanisms across phenotypic categories. When broken down by disease group, dominant variants show notably stronger clustering, with EDC values of 1.31 for CCD, 1.24 for MH, and 1.18 for RRD. In contrast, recessive variants yield an EDC of 1.04, indicative of minimal clustering and consistent with classical loss-of-function mechanisms (57). These findings support the view that most dominant RyR1-related phenotypes are associated with gain-of-function effects, with CCD variants showing the most pronounced spatial clustering. The differences in EDC between phenotypic groups may reflect underlying variation in the strength or specificity of the gain-of-function mechanism involved.

Using spatial clustering as a predictor of pathogenicity

Given the strong clustering observed for dominant RyR1 missense variants, we next explored whether this information could be used to improve the identification of pathogenic variants. Building upon the EDC metric, we introduced a simple spatial clustering feature based on the average distance between a given RyR1 amino acid residue and the *K* nearest other residues that are sites of known pathogenic variants, considering the positions of alpha-carbons in the structure (PDB ID: 7M6A), which we call Spatial Proximity to Disease Variants (SPDV). Since pathogenic variants tend to cluster in three-dimensional space, we reasoned that residues in close proximity to these known sites are more likely to contribute to similar structural or functional disruptions and thus may have a higher likelihood of pathogenicity when mutated. Previous studies have shown that spatial clustering of mutations can help identify functionally important regions or potential driver mutations, particularly in cancer (58, 59), but this has rarely been applied to rare disease variant classification in a clinically interpretable framework (60).

Importantly, while SPDV is based directly on the positions of known pathogenic variants, there is no potential for circularity in our evaluation of its performance. When evaluating the potential pathogenicity of a given mutation at a residue, the calculation only considers the

unique locations of known pathogenic mutations at other residues, *i.e.,* the scoring of a known pathogenic mutation would not be influenced by the fact that it is known to be pathogenic.

In **Figure S3**, we test SPDV for the discrimination between pathogenic and putatively benign missense variants for a range of *K* values. We find the metric is relatively robust to choice of *K*, but the top performance is with *K*=4 (SPDV_4), which achieves a ROC AUC of 0.762. This puts it slightly worse than the top population-free VEPs, but still demonstrates reasonable performance given the orthogonal strategy. An analogous 1D model calculated using distance in primary sequence showed worse performance (ROC AUC: 0.728), demonstrating the importance of considering protein structure. Finally, while our SPDV is based only on the RyR1 subunit structure, considering only intramolecular distances, consideration of intermolecular distances from the full tetramer gave essentially equivalent results (not shown).

Given the overlapping but distinct patterns of clustering observed for the different dominant disorders, and the lack of clustering for recessive variants, we might expect differences in the performance of our spatial clustering model when applied to different mutation classes. Therefore, we repeated the analysis using each of the three dominant disease phenotypes separately **(Figure S4)**. Interestingly, predictive performance improves for the CCD model compared to treating all disease mutations collectively, with a top ROC AUC of 0.806 when using *K*=2. The MH model achieves very similar performance to SPDV calculated using the whole dataset, with a top ROC AUC of 0.760 (*K*=4). The RRD model performs slightly worse with a top ROC AUC of 0.713 (*K*=1). Unsurprisingly, it appears that mutation classes that exhibit a greater degree of clustering, as measured by EDC values, are also better predicted by our SPDV model, especially the CCD phenotype group which also has the highest EDC of 1.31. All the SPDV outputs from our 14 models are available in **Table S3**.

Clinical classification of RyR1 missense variants

To assess the practical utility of our SPDV feature in the context of clinical variant interpretation, we classified missense variants in *RYR1* according to ACMG/AMP guidelines, specifically focusing on the PP3 and BP4 criteria (61, 62). While previous efforts applied genome-wide calibration of VEPs for this purpose (63) , our approach is gene-specific, enabling RYR1-focused calibration of evidence thresholds. Similar to a previously established framework for calibrating VEP scores to evidence strengths (61, 62), we applied a robust kernel density estimation method. Using the VEP scores of pathogenic and putatively benign variants as reference distributions for the calibration, we estimated the positive likelihood ratio, *i.e.*, the odds of pathogenicity for each variant. After determining the

evidence level each VEP reaches for a variant, we focused on the SPDV instance SPDV_4. To avoid potential biases inherent in the use of clinical-trained VEPs, as discussed previously, we compared SPDV_4 to the highest-performing population-free VEP by ROC AUC, PHACT.

The classification results for the two approaches are summarised in **Figure 4**. Interestingly Despite demonstrating a higher discriminatory power by ROC AUC compared to SPDV_4, none of the variants reached higher than moderate evidence for pathogenicity for PHACT. This contrasts with SPDV_4, where 93 of 356 ClinVar pathogenic variants reached the PP3_moderate level. This outcome aligns with the idea that if a variant has an SPDV_4 value below 6.64, the SPDV_4 threshold for moderate pathogenicity level, its four closest pathogenic variants must be in close structural proximity, likely directly spatially adjacent, making it highly probable that the variant itself is also pathogenic. The difference between the two classifiers stems from the observation that PHACT scores of pathogenic variants show a wide overlap with those of benign variants (**Figure 4A**), limiting the magnitude of the estimated likelihood ratios. This finding suggests that ROC AUC alone may not fully capture the clinical utility of a VEP and that metrics accounting for the full score distribution—particularly the relationship between benign and disease-relevant variants—are necessary.

We also examined the proportion of gnomAD variants that reached at least a supporting level of pathogenicity according to each VEP (**Figure 4B**). SPDV_4 assigned supporting evidence to 8.9% of variants, while PHACT assigned nearly twice as many (15%), a significantly higher proportion ($P = 2.2 \times 10^{-16}$, Fisher's exact test). While some recessive or lowly penetrant dominant pathogenic variants may be present in population data, a lower proportion is more consistent with the expectation that this fraction should be minimal.

In ClinVar, SPDV_4 and PHACT assigned at least a supporting level of evidence to 44.7% and 53.3% of variants, respectively (**Figure 4B**). On expert-curated VCEP variants, these proportions were higher, at 49.4% and 64.7%. Given its computational simplicity and performance slightly exceeding that of CPT, we propose SPDV_4 as an orthogonal, structure-based approach for prioritising variants, particularly those with a gain-of-function effect in RyR1. This is further supported by the finding that SPDV_4 identified the largest fraction of CCD variants (**Figure 4B**), which exhibit the highest level of spatial clustering and at least supporting evidence for pathogenicity, as seen in **Figure 3**.

To provide additional clinical value, we explored the potential of SPDV_4 to support PP3/BP4 classifications for ClinVar variants of uncertain significance (VUS). Notably, SPDV_4 provided updated evidence levels for 56.3% (n = 1,852) of these VUS, while the remaining 43.7% (n = 1,436) were classified as "Indeterminate". Among the 1852 classified

variants, 4.44% (n = 146) reached “PP3_moderate”, and 6.66% (n = 219) reached “PP3_supporting”. Conversely, benign classifications included 45.2% (n = 1,487) reaching “BP4_supporting”. The classifications and threshold tables for the full variant dataset are available in **Table S4**.

Conclusions

Although VEPs can be valuable tools for investigating VUSs, they can suffer from biases that can impact their use in clinical settings. In the case of RyR1, the lack of adequate computational VUS interpretation places burden both on clinicians and prospective patients with uncertain clinical diagnoses for an illness in the RyR1 disease spectrum. Due to the phenotypic variation for disease in RyR1 and its extremely long primary sequence, missense variant classification is challenging. In this study, we performed an evaluation of 70 VEPs on RyR1 pathogenic and putatively benign missense variants. Our results suggest that existing computational methods perform poorly in RyR1 variant classification, across all dominant clinical phenotypes.

Previous work from our group investigated the phenomenon of disease variant clustering in protein structures using the EDC metric (19). Building on this, we have here introduced a novel feature based on this phenomenon using mean minimum distances to pathogenic variants in 3D space (SPDV) that resulted in comparable variant classification compared to current VEPs, with the highest performing iteration achieving 0.762 ROC AUC (SPDV_4). Using our clustering metric and structural visualisations of the variants in the RyR1 homotetramer, we demonstrated strong clustering of disease variants in 1D and 3D space. Most notably, CCD variants are extremely clustered at the C terminus of the protein as is shown in the literature (64, 65). These changes are also reflected in the different values for the EDC metric that we calculated for the MH, CCD, RRD, and recessive classes. When compared to Gerasimavicius et al. (19), the MH and CCD variant classes exhibited EDC metrics that were very similar to those of autosomal dominant disease genes associated with dominant-negative and gain-of-function mechanisms. These analyses suggest that distance to pathogenic variants represents a viable and computationally simple strategy for predicting variant pathogenicity. We expect that this could ultimately provide better and more intuitive interpretations of pathogenicity in future analyses of other proteins by avoiding the biases of previous clinical-trained VEPs.

In this study, we classified missense variants in RyR1 from ClinVar using a gene-specific application of odds of pathogenicity thresholds and ACMG/AMP PP3/BP4 evidence levels. Among the population-free VEPs evaluated, PHACT exhibited the highest discriminatory power in distinguishing pathogenic from putatively benign variants. However, compared to

SPDV_4, PHACT assigned supporting evidence to nearly twice as many variants in gnomAD—an unexpectedly high proportion given that truly pathogenic variants should be rare in population databases. While PHACT achieved higher ROC AUC values, its performance was limited by substantial score overlap between pathogenic and benign variants, which constrained its ability to assign higher evidence levels for pathogenicity. This highlights the limitations of relying solely on ROC AUC as a measure of clinical utility. To more effectively assess the relevance of VEPs in variant classification, future approaches should account for the full score distribution and the distinction between benign and pathogenic variants across the entire range of predictions.

Although not intended for direct diagnostic use, SPDV_4 demonstrates substantial clinical utility by providing evidence for 11.1% (n = 365) of ClinVar variants of uncertain significance to at least the "PP3_supporting" level within the ACMG/AMP framework. Its computational simplicity, coupled with its performance that in RYR1 surpasses that of established population-free VEPs such as CPT, underscores its value as a structure-based approach for variant prioritisation. This method is particularly useful for identifying gain-of-function variants in RyR1, providing an orthogonal strategy that complements existing population-free predictors.

Methods

Compilation of variant effect predictor scores

To construct an aggregated set of variant effect predictor results, we used an in-house pipeline to provide these scores for every possible missense variant in RyR1 (25). In total, 70 variant effect predictors were used in the analyses. For DeepSequence, due to the size of the RyR1 protein, it was necessary to split the protein into 7 segments of 800 amino acids (538 for the final segment) with a 50 amino acid overlap. We used Jackhmmer to produce a multiple sequence alignment for each segment from the UniRef100 database with an inclusion threshold of 0.5 bits per residue. DeepSequence was run locally on a GPU for each segment individually to obtain prediction scores for all variants, and mean scores were taken for the overlapping regions.

Variant effect predictor evaluation and calculations

For the evaluation of variant effect predictors, we used RStudio with R version 4.4, along with tidyverse for pre-processing, ROCR for ROC AUC analyses, bio3D and spatstat for the calculation of the spatial clustering features, and ggplot and ggpubr for generating the plots. For these analyses, we removed missing values, duplicates, and made mutually exclusive pathogenic and putatively benign sets.

Spatial clustering feature calculation

The EDC metric was calculated as in Gerasimavicius et al. (19). The spatial clustering model was calculated using both the isolated subunit (considering intramolecular distances only) and using the full tetrameric complexes (considering both intra- and intermolecular distances) using the structure of the rabbit RyR1 tetramer (PDBID: 7M6A), with human variant positions shifted to rabbit positions (66). When using more than one shortest distance, the mean of the 10, 20, 30, 40, or 50 nearest distances to disease variants was used. For spatial clustering in one dimension, the shortest sequence distance between non-self disease variant positions was used.

ACMP/AMP PP3/BP4 classification of variants

The American College of Medical Genetics and Genomics (ACMG) and the Association for Molecular Pathology (AMP) recommend the use of computational predictors as supporting evidence for assessing the pathogenicity or benignity of genetic variants. To classify RyR1 missense variants under the ACMG/AMP PP3/BP4 criteria, we implemented an approach similar to that of Gebbia et al. (2024) (61). For each VEP score, we estimated the likelihood ratio by computing the density ratio between pathogenic and benign variant score distributions. Gaussian kernel density estimates were constructed separately for each class using a bandwidth determined by biased cross-validation. To ensure numerical stability of the ratios, we applied uniform regularisation, setting the penalty to 0.01% of the observed peak density. This process was repeated 1,000 times using bootstrap resampling of the pathogenic and benign variants. The positive likelihood ratio, *i.e.*, odds of pathogenicity, for each score value was computed as the mean of the bootstrap estimates, which were isotonically regressed to ensure monotonicity. The resulting values were compared to threshold values defined by the ACMG/AMP variant classification framework (Tavtigian et al. 2018), assuming a 10% prior probability of pathogenicity. VEP score thresholds for ACMG/AMP evidence levels were determined through linear interpolation between VEP scores and likelihood ratios.

Acknowledgements

We thank Karolina Jackowska for help with compiling the dataset of pathogenic variants, Benjamin Livesey for assistance with the variant effect predictor calculations, Elaine Fletcher for helpful discussions, and Lukas Gerasimavicius for creating the SPDV name and for help with SPDV calculations. This project was supported by the European Research Council (ERC) under the European Union's Horizon 2020 research and innovation programme (grant

agreement No. 101001169), and by core funding from the Medical Research Council to the MRC Human Genetics Unit (MC_UU_00035/9). JAM is a Lister Institute Research Fellow.

References

1. Chen W, Kudryashev M. Structure of RyR1 in native membranes. EMBO reports. 2020;21(5):e49891.

2. Takeshima H, Nishimura S, Matsumoto T, Ishida H, Kangawa K, Minamino N, et al. Primary structure and expression from complementary DNA of skeletal muscle ryanodine receptor. Nature. 1989;339(6224):439-45.

3. Lanner JT. Ryanodine receptor physiology and its role in disease. Calcium Signaling. 2012:217-34.

4. Bai X-C, Yan Z, Wu J, Li Z, Yan N. The Central domain of RyR1 is the transducer for long-range allosteric gating of channel opening. Cell research. 2016;26(9):995-1006.

5. des Georges A, Clarke OB, Zalk R, Yuan Q, Condon KJ, Grassucci RA, et al. Structural basis for gating and activation of RyR1. Cell. 2016;167(1):145-57. e17.

6. Witherspoon JW, Meilleur KG. Review of RyR1 pathway and associated pathomechanisms. Acta neuropathologica communications. 2016;4(1):1-20.

7. Murayama T, Kurebayashi N, Ogawa H, Yamazawa T, Oyamada H, Suzuki J, et al. Genotype–phenotype correlations of malignant hyperthermia and central core disease mutations in the central region of the RYR1 channel. Human Mutation. 2016;37(11):1231-41.

8. Hernandez-Ochoa EO, Pratt SJ, Lovering RM, Schneider MF. Critical role of intracellular RyR1 calcium release channels in skeletal muscle function and disease. Frontiers in physiology. 2016;6:420.

9. Chen W, Koop A, Liu Y, Guo W, Wei J, Wang R, et al. Reduced threshold for store overload-induced Ca2+ release is a common defect of RyR1 mutations associated with malignant hyperthermia and central core disease. Biochemical Journal. 2017;474(16):2749-61.

10. Dirksen RT, Avila G. Distinct effects on Ca2+ handling caused by malignant hyperthermia and central core disease mutations in RyR1. Biophysical journal. 2004;87(5):3193-204.

11. Zhou H, Rokach O, Feng L, Munteanu I, Mamchaoui K, Wilmshurst JM, et al. RyR 1 Deficiency in Congenital Myopathies Disrupts Excitation–Contraction Coupling. Human mutation. 2013;34(7):986-96.

12. Scacheri P, Hoffman E, Fratkin J, Semino–Mora C, Senchak A, Davis M, et al. A novel ryanodine receptor gene mutation causing both cores and rods in congenital myopathy. Neurology. 2000;55(11):1689-96.

13. Alkhunaizi E, Shuster S, Shannon P, Siu VM, Darilek S, Mohila CA, et al. Homozygous/compound heterozygote RYR1 gene variants: expanding the clinical spectrum. American Journal of Medical Genetics Part A. 2019;179(3):386-96.

14. Kruijt N, den Bersselaar LV, Snoeck M, Kramers K, Riazi S, Bongers C, et al. RYR1-related rhabdomyolysis: a spectrum of hypermetabolic states due to ryanodine receptor dysfunction. Current Pharmaceutical Design. 2022;28(1):2-14.

15. Snoeck M, Van Engelen B, Küsters B, Lammens M, Meijer R, Molenaar J, et al. RYR 1-related myopathies: a wide spectrum of phenotypes throughout life. European journal of neurology. 2015;22(7):1094-112.

16. Lawal TA, Todd JJ, Witherspoon JW, Bönnemann CG, Dowling JJ, Hamilton SL, et al. Ryanodine receptor 1-related disorders: an historical perspective and proposal for a unified nomenclature. Skeletal Muscle. 2020;10(1):1-16.

17. Moulds R, Denborough M. Biochemical basis of malignant hyperpyrexia. Br Med J. 1974;2(5913):241-4.

18. Livesey BJ, Marsh JA. Interpreting protein variant effects with computational predictors and deep mutational scanning. Disease Models & Mechanisms. 2022;15(6):dmm049510.

19. Gerasimavicius L, Livesey BJ, Marsh JA. Loss-of-function, gain-of-function and dominant-negative mutations have profoundly different effects on protein structure. Nature communications. 2022;13(1):1-15.

20. Cherednichenko G, Ward CW, Feng W, Cabrales E, Michaelson L, Samso M, et al. Enhanced excitation-coupled calcium entry in myotubes expressing malignant hyperthermia mutation R163C is attenuated by dantrolene. Molecular pharmacology. 2008;73(4):1203-12.

21. Iyer KA, Hu Y, Nayak AR, Kurebayashi N, Murayama T, Samsó M. Structural mechanism of two gain-of-function cardiac and skeletal RyR mutations at an equivalent site by cryo-EM. Science advances. 2020;6(31):eabb2964.

22. Yang T, Esteve E, Pessah IN, Molinski TF, Allen PD, López JR. Elevated resting [Ca2+] i in myotubes expressing malignant hyperthermia RyR1 cDNAs is partially restored by modulation of passive calcium leak from the SR. American Journal of Physiology-Cell Physiology. 2007;292(5):C1591-C8.

23. Badonyi M, Marsh JA. Proteome-scale prediction of molecular mechanisms underlying dominant genetic diseases. Plos one. 2024;19(8):e0307312.

24. Johnston JJ, Dirksen RT, Girard T, Hopkins PM, Kraeva N, Ognoon M, et al. Updated variant curation expert panel criteria and pathogenicity classifications for 251 variants for RYR1-related malignant hyperthermia susceptibility. Human Molecular Genetics. 2022;31(23):4087-93.

25. Livesey BJ, Marsh JA. Using deep mutational scanning to benchmark variant effect predictors and identify disease mutations. Molecular systems biology. 2020;16(7):e9380.

26. Williamson KA, Hall HN, Owen LJ, Livesey BJ, Hanson IM, Adams G, et al. Recurrent heterozygous PAX6 missense variants cause severe bilateral microphthalmia via predictable effects on DNA–protein interaction. Genetics in Medicine. 2020;22(3):598-609.

27. Gerasimavicius L, Liu X, Marsh JA. Identification of pathogenic missense mutations using protein stability predictors. Scientific reports. 2020;10(1):1-10.

28. Young SL, Stanton CM, Livesey BJ, Marsh JA, Cackett PD. Novel biallelic USH2A variants in a patient with usher syndrome type IIA-a case report. BMC ophthalmology. 2022;22(1):1-9.

29. Livesey BJ, Marsh JA. The properties of human disease mutations at protein interfaces. PLOS Computational Biology. 2022;18(2):e1009858.

30. Attard TJ, Welburn JP, Marsh JA. Understanding molecular mechanisms and predicting phenotypic effects of pathogenic tubulin mutations. PLOS Computational Biology. 2022;18(10):e1010611.

31. Livesey BJ, Marsh JA. Updated benchmarking of variant effect predictors using deep mutational scanning. Molecular Systems Biology. 2023;n/a(n/a):e11474.

32. Wu Y, Liu H, Li R, Sun S, Weile J, Roth FP. Improved pathogenicity prediction for rare human missense variants. The American Journal of Human Genetics. 2021;108(10):1891-906.

33. Koch L. Exploring human genomic diversity with gnomAD. Nature Reviews Genetics. 2020;21(8):448-.

34. Huang J, Ling CX. Using AUC and accuracy in evaluating learning algorithms. IEEE Transactions on knowledge and Data Engineering. 2005;17(3):299-310.

35. Livesey BJ, Marsh JA. Variant effect predictor correlation with functional assays is reflective of clinical classification performance. bioRxiv. 2024:2024.05. 12.593741.

36. Srivastava N, Hinton G, Krizhevsky A, Sutskever I, Salakhutdinov R. Dropout: a simple way to prevent neural networks from overfitting. The journal of machine learning research. 2014;15(1):1929-58.

37. Schaafsma GC, Vihinen M. Representativeness of variation benchmark datasets. BMC bioinformatics. 2018;19(1):1-19.

38. Grimm DG, Azencott CA, Aicheler F, Gieraths U, MacArthur DG, Samocha KE, et al. The evaluation of tools used to predict the impact of missense variants is hindered by two types of circularity. Human mutation. 2015;36(5):513-23.

39. Meier J, Rao R, Verkuil R, Liu J, Sercu T, Rives A. Language models enable zero-shot prediction of the effects of mutations on protein function. Advances in Neural Information Processing Systems. 2021;34:29287-303.

40. Livesey BJ, Marsh JA. Advancing variant effect prediction using protein language models. Nature genetics. 2023;55(9):1426-7.

41. Cheng J, Novati G, Pan J, Bycroft C, Žemgulytė A, Applebaum T, et al. Accurate proteome-wide missense variant effect prediction with AlphaMissense. Science. 2023;381(6664):eadg7492.

42. Pathak AK, Bora N, Badonyi M, Livesey BJ, Consortium SKH, Ngeow J, et al. Pervasive ancestry bias in variant effect predictors. bioRxiv. 2024:2024.05. 20.594987.

43. Feng BJ. PERCH: a unified framework for disease gene prioritization. Human mutation. 2017;38(3):243-51.

44. Kuru N, Dereli O, Akkoyun E, Bircan A, Tastan O, Adebali O. PHACT: phylogeny-aware computing of tolerance for missense mutations. Molecular Biology and Evolution. 2022;39(6):msac114.

45. Jagota M, Ye C, Albors C, Rastogi R, Koehl A, Ioannidis N, et al. Cross-protein transfer learning substantially improves disease variant prediction. Genome Biology. 2023;24(1):182.

46. Riesselman AJ, Ingraham JB, Marks DS. Deep generative models of genetic variation capture the effects of mutations. Nature methods. 2018;15(10):816-22.

47. Gerasimavicius L, Teichmann SA, Marsh JA. Leveraging protein structural information to improve variant effect prediction. Current opinion in structural biology. 2025;92:103023.

48. Birolo G, Benevenuta S, Fariselli P, Capriotti E, Giorgio E, Sanavia T. Protein stability perturbation contributes to the loss of function in haploinsufficient genes. Frontiers in Molecular Biosciences. 2021;8:620793.

49. Schymkowitz J, Borg J, Stricher F, Nys R, Rousseau F, Serrano L. The FoldX web server: an online force field. Nucleic acids research. 2005;33(suppl_2):W382-W8.

50. Gerasimavicius L, Livesey BJ, Marsh JA. Correspondence between functional scores from deep mutational scans and predicted effects on protein stability. Protein Science. 2023:e4688.

51. Ponting CP. Novel repeats in ryanodine and IP3 receptors and protein O-mannosyltransferases. Trends in biochemical sciences. 2000;25(2):47-50.

52. Todd JJ, Sagar V, Lawal TA, Allen C, Razaqyar MS, Shelton MS, et al. Correlation of phenotype with genotype and protein structure in RYR1-related disorders. Journal of neurology. 2018;265:2506-24.

53. Zalk R, Clarke OB, Des Georges A, Grassucci RA, Reiken S, Mancia F, et al. Structure of a mammalian ryanodine receptor. Nature. 2015;517(7532):44-9.

54. Murayama T, Ogawa H, Kurebayashi N, Ohno S, Horie M, Sakurai T. A tryptophan residue in the caffeine-binding site of the ryanodine receptor regulates Ca2+ sensitivity. Communications biology. 2018;1(1):98.

55. Kushnir A, Todd JJ, Witherspoon JW, Yuan Q, Reiken S, Lin H, et al. Intracellular calcium leak as a therapeutic target for RYR1-related myopathies. Acta neuropathologica. 2020;139:1089-104.

56. Amburgey K, Bailey A, Hwang JH, Tarnopolsky MA, Bonnemann CG, Medne L, et al. Genotype-phenotype correlations in recessive RYR1-related myopathies. Orphanet journal of rare diseases. 2013;8(1):1-12.

57. Backwell L, Marsh JA. Diverse Molecular Mechanisms Underlying Pathogenic Protein Mutations: Beyond the Loss-of-Function Paradigm. Annual Review of Genomics and Human Genetics. 2022;23.

58. Kamburov A, Lawrence MS, Polak P, Leshchiner I, Lage K, Golub TR, et al. Comprehensive assessment of cancer missense mutation clustering in protein structures. Proceedings of the National Academy of Sciences. 2015;112(40):E5486-E95.

59. Chillón-Pino D, Badonyi M, Semple CA, Marsh JA. Protein structural context of cancer mutations reveals molecular mechanisms and candidate driver genes. Cell Reports. 2024;43(11).

60. Baugh EH, Simmons-Edler R, Müller CL, Alford RF, Volfovsky N, Lash AE, et al. Robust classification of protein variation using structural modelling and large-scale data integration. Nucleic acids research. 2016;44(6):2501-13.

61. Gebbia M, Zimmerman D, Jiang R, Nguyen M, Weile J, Li R, et al. A missense variant effect map for the human tumor-suppressor protein CHK2. The American Journal of Human Genetics. 2024;111(12):2675-92.

62. van Loggerenberg W, Sowlati-Hashjin S, Weile J, Hamilton R, Chawla A, Sheykhkarimli D, et al. Systematically testing human HMBS missense variants to reveal mechanism and pathogenic variation. The American Journal of Human Genetics. 2023;110(10):1769-86.

63. Pejaver V, Byrne AB, Feng B-J, Pagel KA, Mooney SD, Karchin R, et al. Calibration of computational tools for missense variant pathogenicity classification and ClinGen

recommendations for PP3/BP4 criteria. The American Journal of Human Genetics. 2022;109(12):2163-77.

64. Davis M, Haan E, Jungbluth H, Sewry C, North K, Muntoni F, et al. Principal mutation hotspot for central core disease and related myopathies in the C-terminal transmembrane region of the RYR1 gene. Neuromuscular disorders. 2003;13(2):151-7.

65. Shepherd S, Ellis F, Halsall J, Hopkins P, Robinson R. RYR1 mutations in UK central core disease patients: more than just the C-terminal transmembrane region of the RYR1 gene. Journal of Medical Genetics. 2004;41(3):e33-e.

66. Melville Z, Kim K, Clarke OB, Marks AR. High-resolution structure of the membrane-embedded skeletal muscle ryanodine receptor. Structure. 2022;30(1):172-80. e3.

Figures

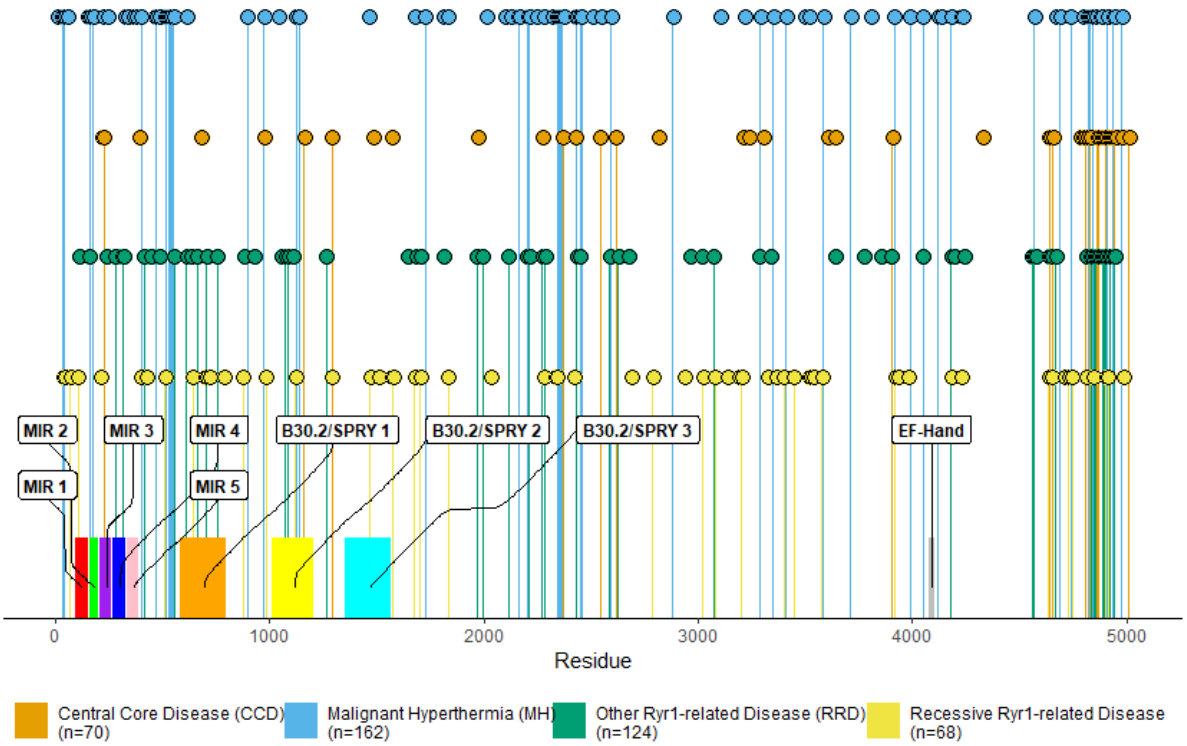

Figure 1: Disease-associated RyR1 mutations cluster in linear space. Lollipop plot of RYR1 variant positions by disease across the amino acid sequence with domains indicated from UniProt (ID: P21817).

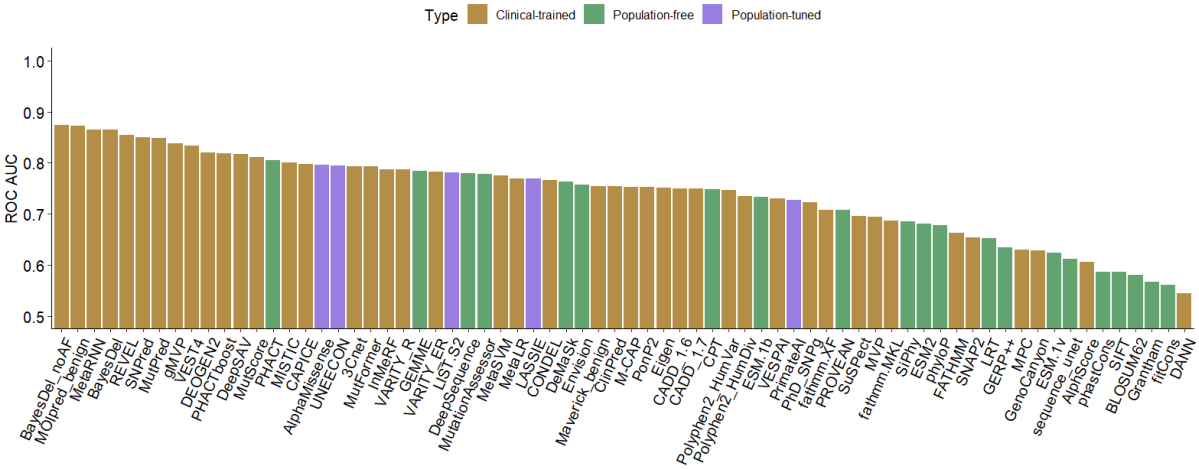

Figure 2: Performance of VEPs for the discrimination between of pathogenic and putatively benign RyR1 variants. Bar plot showing the performance using ROC AUC (area under the receiver operating characteristic curve) for all the VEPs used in this study when evaluating pathogenicity of the variant dataset. VEPs are coloured by class: clinical-trained (brown), population-free (green) and population-tuned (violet).

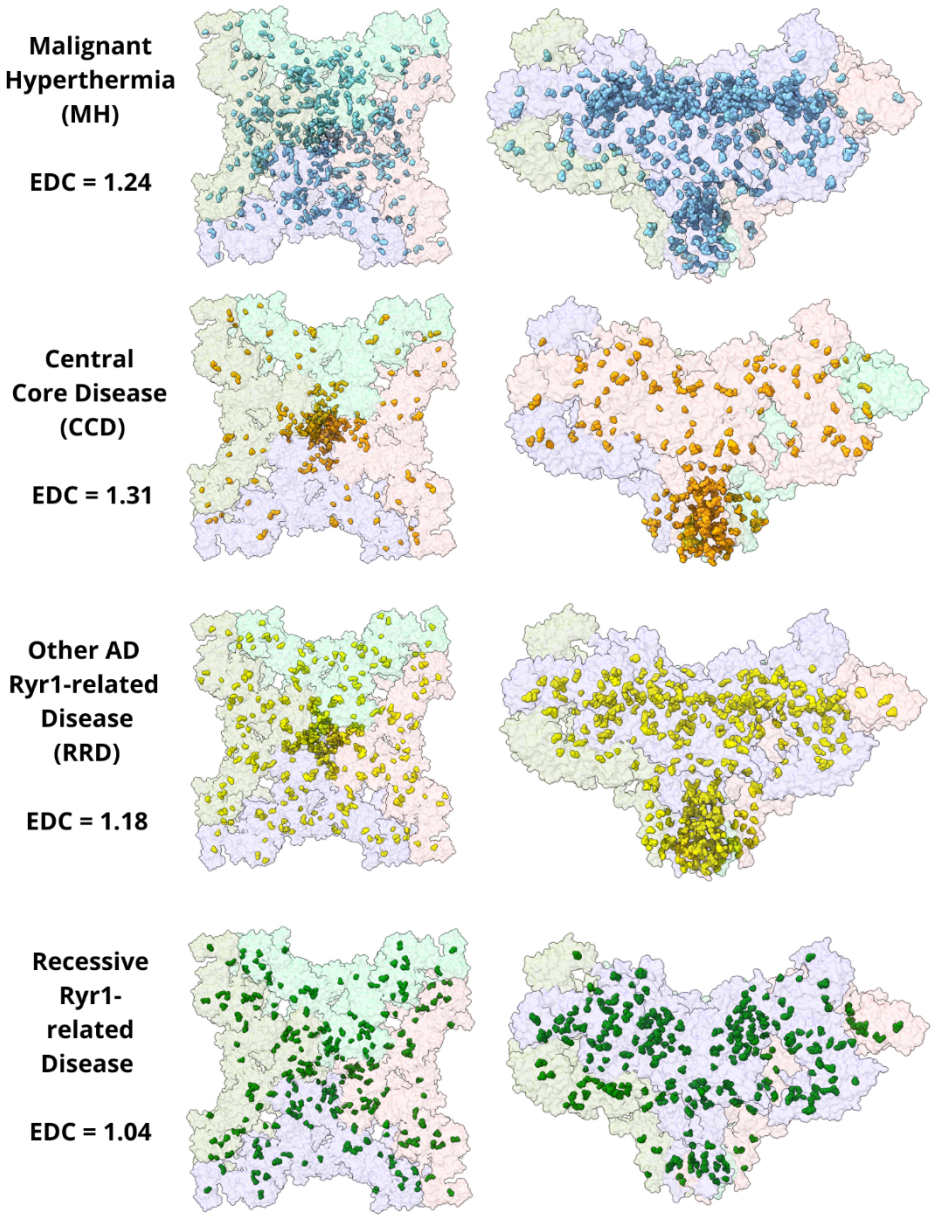

Figure 3: Clustering of pathogenic missense variants within the tetrameric structure of RyR1. The structure of rabbit RyR1 (PDB ID: 7M6A) is used, variant positions shifted with respect to the human sequence. Pathogenic missense variants are highlighted and coloured (blue: MH, malignant hyperthermia; orange: CCD, central core disease; yellow: RRD, other AD RYR1-related diseases, green: AR RYR1-related diseases (recessive). These images show similar patterns as in Figure 1, with missense variants appearing across the sequence in the top and side views.

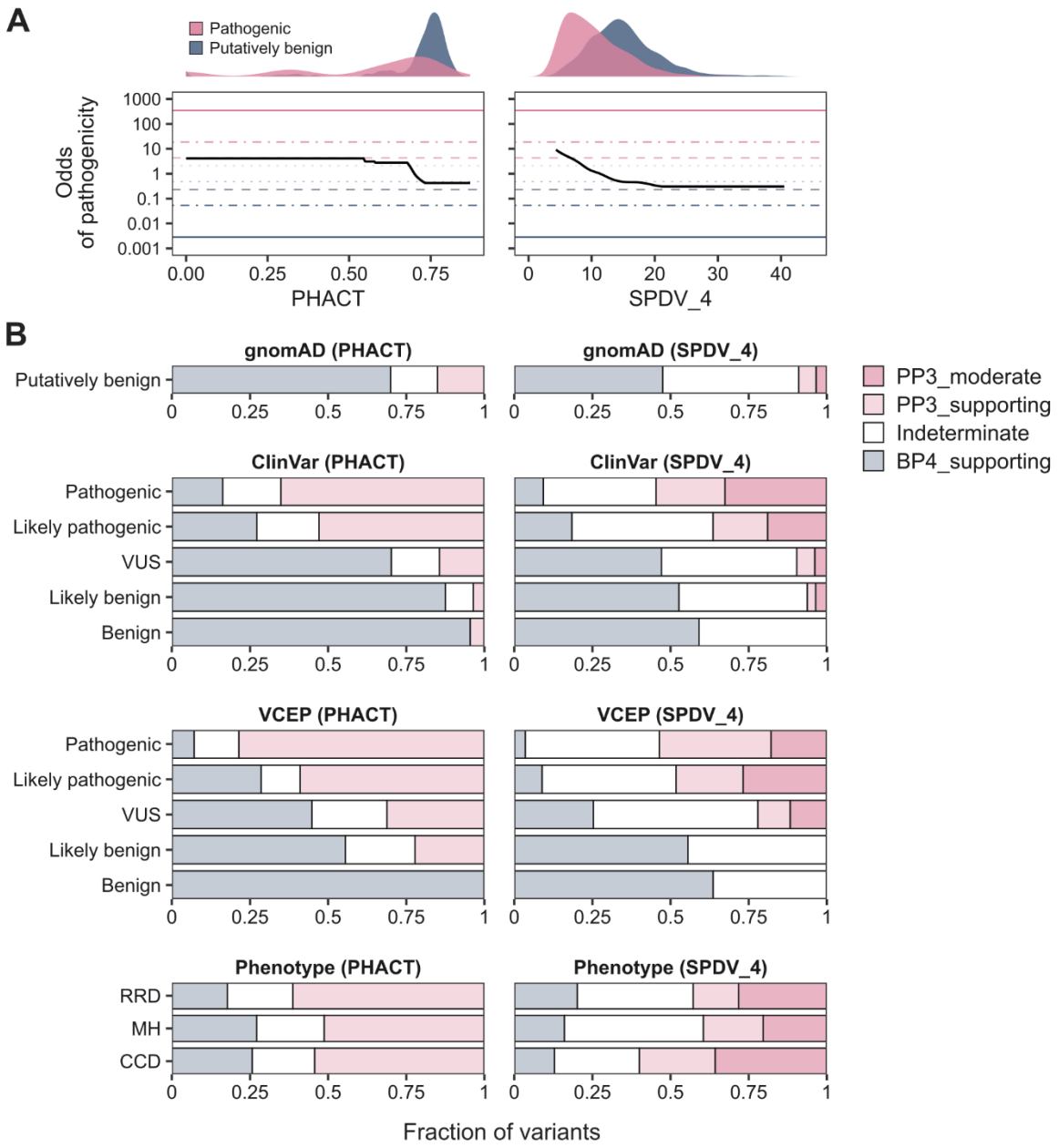

Figure 4: Comparison of ACMG/AMP variant classification outcomes for RyR1 missense variants between PHACT and SPDV_4. (A) PHACT and SPDV_4 plotted against their odds of pathogenicity values. Horizontal lines show the odds of pathogenicity thresholds corresponding to the PP3/BP4 evidence levels, which were derived from the very strong threshold for pathogenicity based on a 10% prior. Density plots on the top show the distribution of putatively benign (gnomAD v4.1) and pathogenic (ClinVar P/LP) variants. **(B)** Composition of PP3/BP4 evidence classes reached by PHACT and SPDV_4 in the following missense variant categories: gnomAD v4.1, ClinVar, Variant Curation Expert Panel (VCEP), and Phenotype, which includes the dominant phenotypes RRD, MH and CCD.

Supplementary Figures

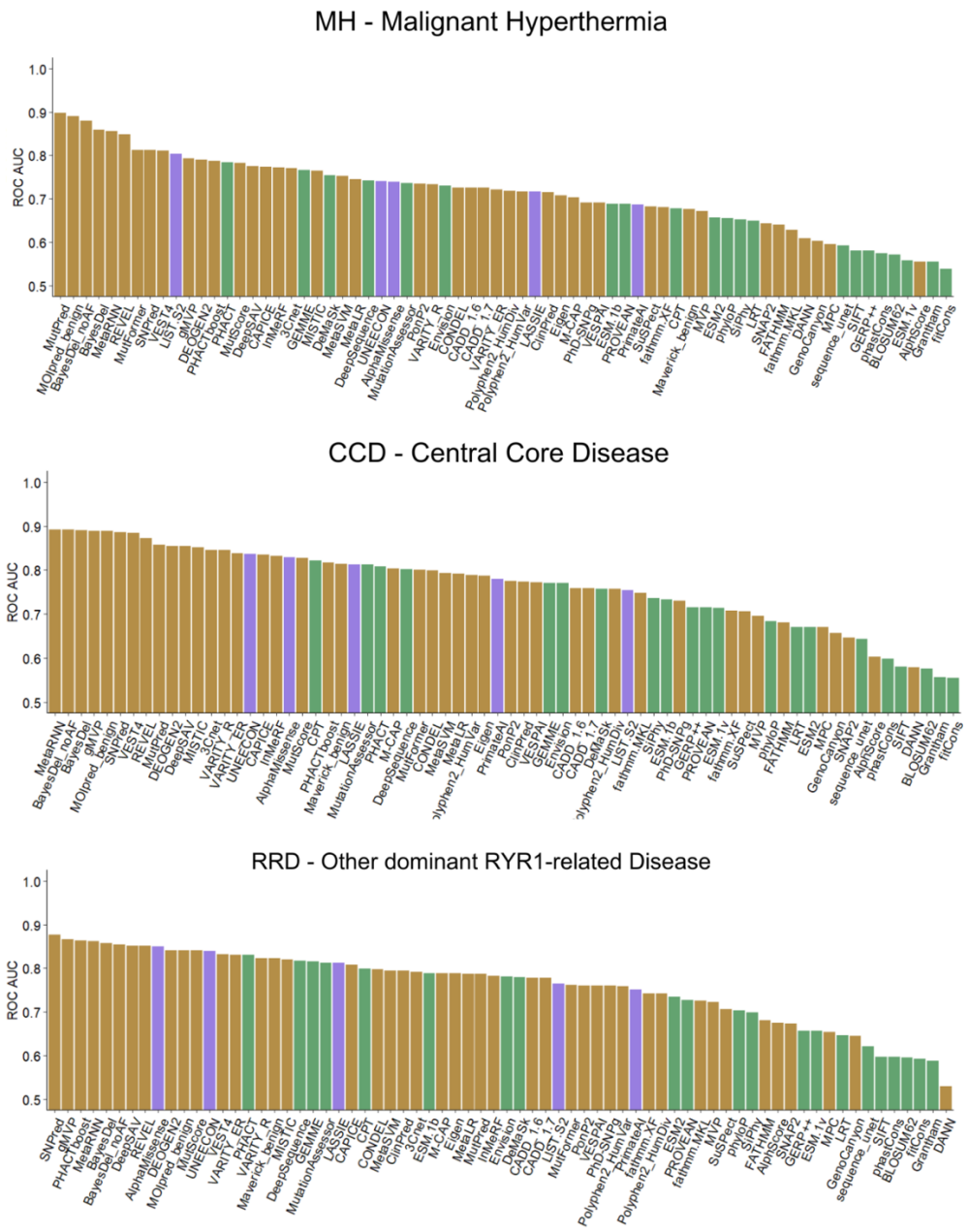

Figure S1: VEP performance for the identification of pathogenic RyR1 variants by phenotypic group. Bar plot showing the performance using ROC AUC (area under the receiver operating characteristic curve) for all the VEPs used in this study when evaluating pathogenicity of variants by the MH (malignant hyperthermia), CCD (central core disease), and RRD (other dominant RYR1-related disease) groups when compared to putatively benign variants. VEPs are coloured by class: clinical-trained (brown), population-free (green) and population-tuned (violet).

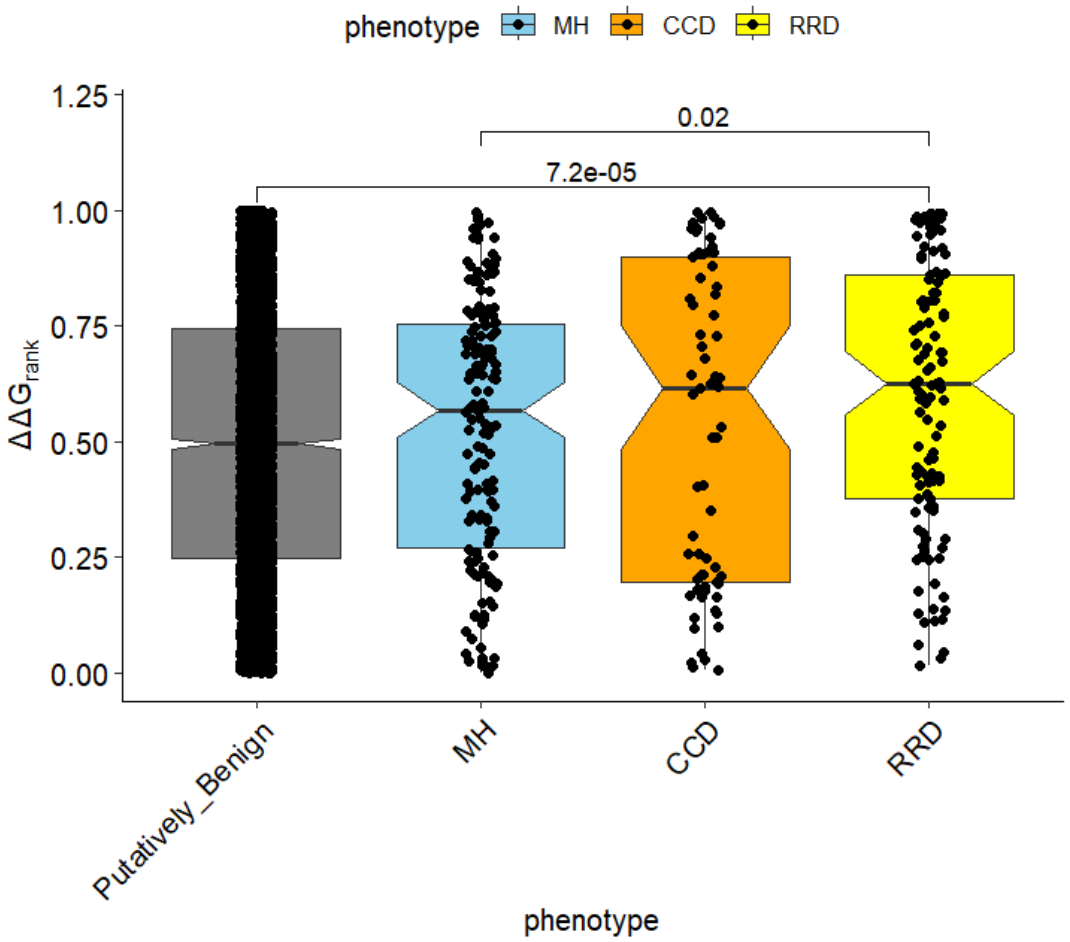

Figure S2: Comparison of $\Delta\Delta G_{rank}$ values from missense variants associated with different RYR1 phenotypic groups. $\Delta\Delta G_{rank}$ is a recently introduced rank-normalised representation of $|\Delta\Delta G|$ that improves visual comparisons (10.1016/j.celrep.2024.114905).

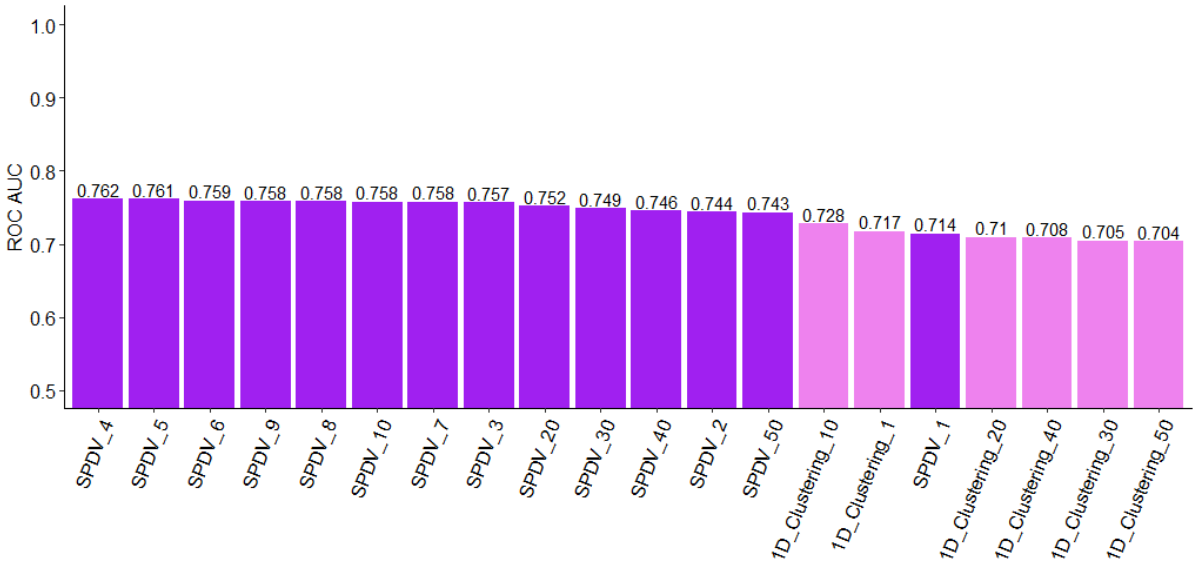

Figure S3: SPDV_4 is the top performing SPDV instance. The performance of different SPDV instances using the 3D protein structure and *K*=1-10, 20, 30, 40, and 50 nearest disease variant distances does not vary substantially. We therefore used SPDV_4 for analyses following this evaluation. Using sequence distances (1D as opposed to 3D), showed that the instances we tested performed with lower ROC AUC performance other than SPDV_1 (**Table S3**).

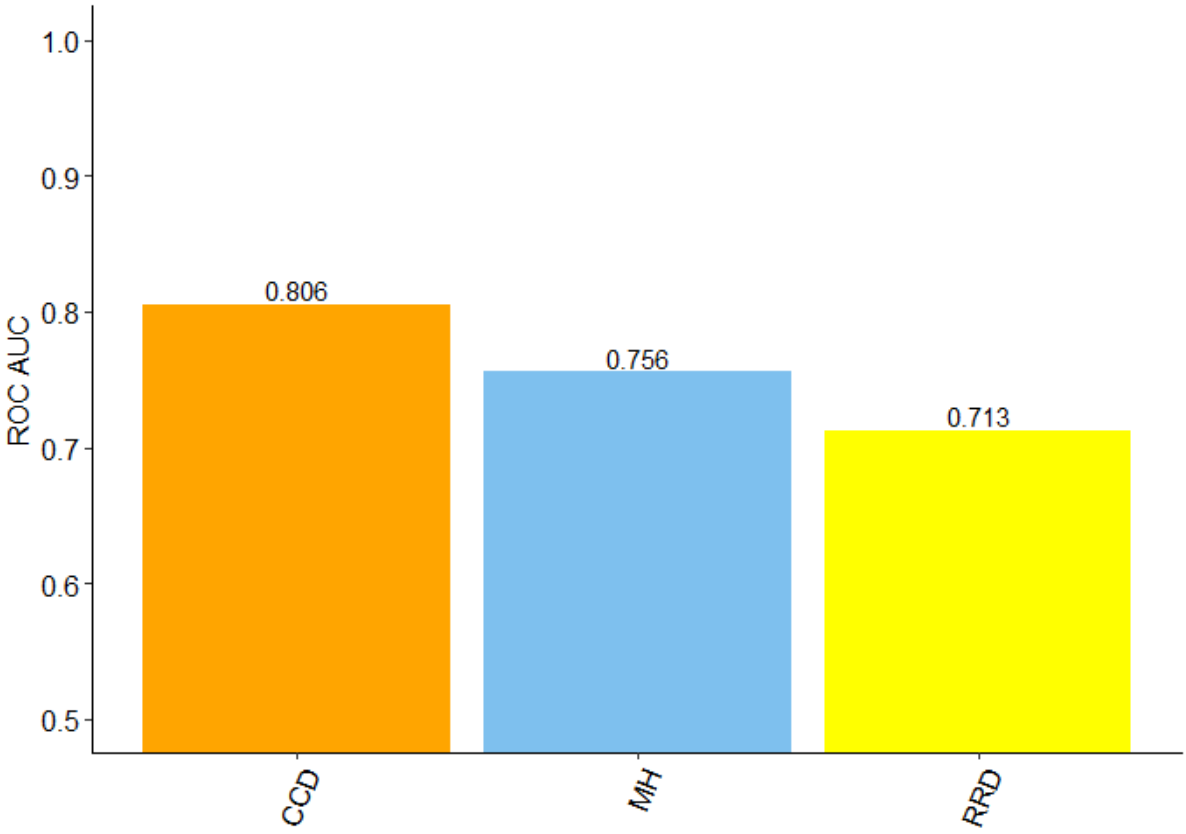

Figure S4: Performance of the top performing SPDV instances by phenotypic group. Predictive performance improves for the CCD model compared to treating all disease mutations collectively, with a top ROC AUC of 0.806 (*K*=2). The MH model achieves very similar performance to SPDV calculated using the whole dataset, with a top ROC AUC of 0.760 (*K*=4). The RRD model performs slightly worse with a top ROC AUC of 0.713 (*K*=1).

Supplementary Tables

Table S1: Pathogenic missense variants and their sources. This table includes all the variants gathered from the various databases and literature searches we used to gather as many RYR1 pathogenic missense variants as possible. Here we have provided the 'Missense Variants' tab, which includes the variants and their sources, as well as the 'Literature' tab, which contains the paper references for the relevant variants.

Table S2: RYR1 complete dataset and ROC AUC evaluations using the full dataset and phenotype-specific sets. This table includes the pathogenic missense variants together with the putatively benign variants from gnomAD, along with their associated VEP scores. Here we have provided the 'Complete Dataset' tab, which includes all the aforementioned data, as well as the 'Complete Dataset', 'AUROC' and 'By phenotype', 'AUROC' tabs, which contain the results of the VEP ROC AUC evaluations for these sets.

Table S3: SPDV values for all residues in RYR1 and ROC AUC evaluations using the full dataset and phenotype-specific sets. This table includes all the SPDV values calculated using K=1-10,20,30,40, and 50 for all the residues in RYR1. Here we have provided the 'SPDV 1-50' tab, which includes all the aforementioned data, as well as the 'SPDV Complete Dataset', 'AUROC' and 'SPDV By phenotype', 'AUROC tabs', which contain the results of the SPDV ROC AUC evaluations for these sets.

Table S4: ACMG values and ACMG thresholds for VEPs. This contains the score intervals for the given ACMG/AMP PP3/BP4 evidence strengths.